International Journal of Fracture **51:** 175–186, 1991.
Z.P. Bažant (ed.), Current Trends in Concrete Fracture Research.

Size-scale transition from ductile to brittle failure: structural response vs. crack growth resistance curve

ALBERTO CARPINTERI
Politecnico di Torino, Department of Structural Engineering, 10129 Torino, Italy

Received 11 June 1990; accepted 11 November 1990

Abstract. The concept of brittleness number is revised emphasizing the distinction between a stress-intensification treatment and an energy treatment. In the case of power-law hardening materials the relation between plastic stress-intensity factor and J-integral is translated into a relation between stress brittleness number and energy brittleness number. The structural response generally depends on both such numbers and, therefore, is not physically similar when varying the size-scale of the body. A connection is then established between structural response and crack growth resistance curve, the relevant parameters of a scale-invariant J-resistance curve being related to the energy brittleness number.

1. Introduction

The *structural response* is not physically similar when varying the size-scale of the body. A transition is experimentally evident from plastic collapse to brittle failure, passing through hardening, softening and snap-back behaviour. At the same time, the *crack behaviour* undergoes the same transition, from slow and stable growth to fast and unstable propagation. Both structural response and crack behaviour depend also on the controlling parameter. If the feed-back quantity is the load, only global hardening behaviours may be detected; when the feed-back quantity is the loading point displacement, both hardening and softening behaviours may be controlled; when the feed-back quantity is the crack mouth opening displacement, (*CMOD*), even the snap-back or catastrophic branches can be captured.

In the present paper, a connection is established between *structural analysis* and the *crack growth resistance concept*. When the (*energy*) *brittleness number* s_E^* is lower than the intercept $\tilde{J}_0$ of the scale-invariant J-resistance curve, the structural response presents a sharp cusp catastrophe and the virtual J-resistance curve presents values always higher than the critical J_{IC}. On the other hand, when s_E^* is higher than $\tilde{J}_0 + \tilde{J}'(\xi - \xi_0)$, where $\tilde{J}'$ is the slope of the scale-invariant J-resistance curve, and ξ is the relative crack length (ξ_0 = initial value), the structural response is very ductile and the J-resistance curve presents values always lower than the critical J_{IC}.

The brittleness number concept was proposed by the writer with reference to the stress-intensity factor for linear elastic materials [1–7] as well as for power-law hardening materials [8]. Subsequently, the concept was extended with reference to the strain energy release rate [9–15]. Herein it will be applied to the J-resistance curve. The same concept was proposed by the writer for reinforced concrete [16–19] and by Bažant for aggregate materials [20, 21].

It will be demonstrated that the brittleness number based on the stress-intensity factor is connected with the brittleness number based on the strain energy release rate in the case

of linear elastic materials. Similarly, the brittleness number based on the plastic stress-intensity factor is connected with the brittleness number based on the J-integral in the case of power-law hardening materials. In general, the structural response depends on both these brittleness numbers, independent of the constitutive law of the material. An exception is provided in the case of the three point bending specimen of linear elastic material [12].

2. Scale effect on the structural response

2.1. Strain-hardening material

Let us consider a non-linear material with a double constitutive law in tension (Fig. 1). The former law (Fig. 1a) is a Ramberg-Osgood strain-hardening power-law:

$$\tilde{\varepsilon} = \tilde{\sigma}^n, \tag{1}$$

where $\tilde{\varepsilon}$ and $\tilde{\sigma}$ are non-dimensionalized with respect to the corresponding maximum values of strain and stress, ε_y and σ_y, and n is the Ramberg-Osgood exponent, $1 \leqslant n < \infty$. The latter law (Fig. 1b) is a strain-softening power-law of crack opening displacement, w, and stress, σ:

$$\tilde{w} = (1 - \tilde{\sigma})^{n'}, \tag{2}$$

where $\tilde{w}$ is non-dimensionalized with respect to the value w_c, beyond which the interaction between the crack surfaces vanishes, and n' is a softening exponent, $1 \leqslant n' < \infty$.

Let us assume that a solid body of the material described above is loaded by a concentrated force P, δ being the displacement of the force in its direction (Fig. 2). The functional relationship between force and displacement can appear as not fulfilling the monodromy condition, when snap-back instability is present (Fig. 3). On the other hand, such a relationship can always be

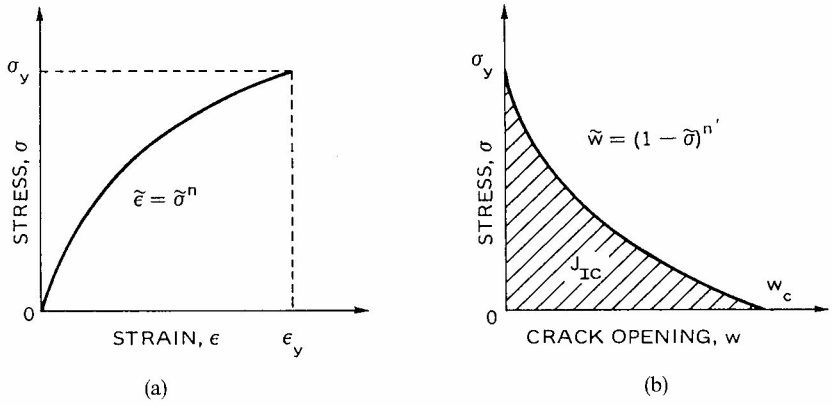

Fig. 1. Non-linear constitutive laws.

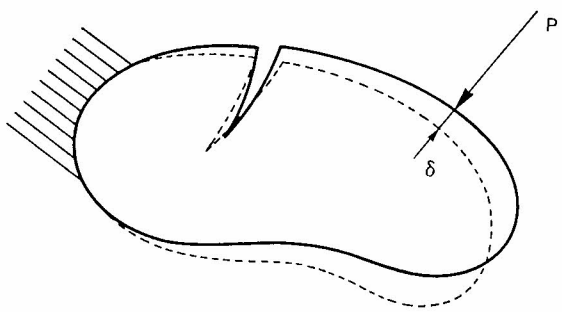

Fig. 2. Cracked body.

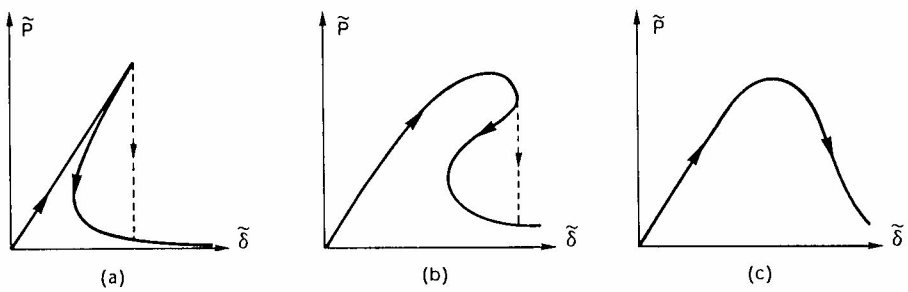

Fig. 3. Load vs. deflection paths: catastrophic (a), snap-back (b) and softening (c) behaviour.

put into the following general form [22]:

$$\pi\left(\frac{P}{\sigma_y b^2}, \frac{\delta}{b}; \varepsilon_y, \frac{J_{IC}}{\sigma_y b}, n, n'; \xi_i\right) = 0, \tag{3}$$

according to Buckingham's Theorem for physical similitude and scale modelling. In (3), b is a characteristic dimension of the body, J_{IC} is the area under the curve σ vs w (Fig. 1b), usually called the J-integral [23], ξ_i are the geometrical ratios necessary to describe the shape of the body.

If we fix the shape of the body and the shape of the non-linear constitutive diagrams in Fig. 1, the functional relationship (3) becomes

$$\pi(\tilde{P}, \tilde{\delta}; \varepsilon_y, s_E^*) = 0, \tag{4}$$

where $\tilde{P}$ is the dimensionless load, $\tilde{\delta}$ is the dimensionless displacement, and

$$s_E^* = \frac{J_{IC}}{\sigma_y b}, \tag{5}$$

is the *(energy) brittleness number* in the case of Ramberg-Osgood material.

The stress, strain and displacement fields at the crack tip present the following forms respectively [24, 25, 8]:

$$\sigma_{ij} = K_{\mathrm{I}}^{*} r^{-1/(n+1)} \tilde{\sigma}_{ij}(\theta), \tag{6a}$$

$$\varepsilon_{ij} = \varepsilon_y \left(\frac{K_{\mathrm{I}}^{*}}{\sigma_y} \right)^{n} r^{-n/(n+1)} \tilde{\varepsilon}_{ij}(\theta), \tag{6b}$$

$$u_i = \varepsilon_y \left(\frac{K_{\mathrm{I}}^{*}}{\sigma_y} \right)^{n} r^{1/(n+1)} \tilde{u}_i(\theta), \tag{6c}$$

where K_{I}^{*} is the plastic stress-intensity factor, r is the radial coordinate, θ is the angular coordinate, and $\tilde{\sigma}_{ij}$, $\tilde{\varepsilon}_{ij}$, $\tilde{u}_i$ are non-dimensional functions of θ.

When $n \to \infty$ (rigid-plastic material) the stress-singularity tends to disappear, while the displacement tends to become only a function of θ.

It is possible to relate the plastic stress-intensity factor K_{I}^{*} to the J-integral

$$J_{\mathrm{I}} = \int_{\mathscr{C}} W \, \mathrm{d}y - \sigma_{ij} n_j u_{i,x} \, \mathrm{d}l. \tag{7}$$

Namely, performing the integral along a circumference $\mathscr{C}$ centered in the crack tip, sufficiently small so that such a zone is dominated by the plastic singularity, yields [25, 8]

$$J_{\mathrm{I}} = \left(\frac{K_{\mathrm{I}}^{*}}{\sigma_y} \right)^{n+1} I_n \sigma_y \varepsilon_y, \tag{8}$$

where I_n is a well-known dimensionless function of n. The relation between J_{I} and K_{I}^{*} can be stated in the following form:

$$K_{\mathrm{I}}^{*} = \sigma_y \left(\frac{J_{\mathrm{I}}}{I_n \sigma_y \varepsilon_y} \right)^{1/(n+1)}. \tag{9}$$

If the (*stress*) *brittleness number* in the general case of Ramberg-Osgood material is defined as [8]

$$s^{*} = \frac{K_{\mathrm{IC}}^{*}}{\sigma_y b^{1/(n+1)}}, \tag{10}$$

where K_{IC}^{*} is the critical value of the plastic stress-intensity factor K_{I}^{*}, from (5), (9) and (10) it is easy to obtain

$$s_E^{*} = I_n \varepsilon_y s^{*(n+1)}. \tag{11}$$

Equation (11) represents the relation between *energy brittleness number* and *stress brittleness number* in terms of the ultimate strain ε_y and the Ramberg-Osgood exponent n.

Equation (11) permits the transformation from (4) to

$$\bar{\pi}(\tilde{P}, \tilde{\delta}; s^*, s_E^*) = 0. \tag{12}$$

Equation (12) states that the $\tilde{P}$ vs $\tilde{\delta}$ path is the same if both the brittleness numbers s^* and s_E^* do not change. The reverse is not true.

2.2. *Linear-elastic material*

In the limit case $n = 1$, the Ramberg-Osgood material becomes linear-elastic (Fig. 4a), and the ratio

$$\sigma_y/\varepsilon_y = \sigma_u/\varepsilon_u = E, \tag{13}$$

represents the Young's modulus of the material.

On the other hand, for $n' = 1$, even the softening cohesive law is linear (Fig. 4b), with

$$J_{IC} = \mathcal{G}_{IC} = \mathcal{G}_F = \tfrac{1}{2}\sigma_u w_c. \tag{14}$$

If the ascending σ vs. ε law is linear elastic, the critical value of the J-integral must be equal to the critical value of the strain energy release rate, $\mathcal{G}_{IC}$, or to the fracture energy $\mathcal{G}_F$.

The functional relationship (3) between force and displacement (Figs. 2 and 3) in the case of linear-elastic material takes the particular form:

$$\pi\left(\frac{P}{\sigma_u b^2}, \frac{\delta}{b}; \nu, \varepsilon_u, \frac{\mathcal{G}_{IC}}{\sigma_u b}; \xi_i\right) = 0, \tag{15}$$

where ν is the Poisson ratio. If we fix the shape of the body, (15) becomes

$$\pi(\tilde{P}, \tilde{\delta}; \nu, \varepsilon_u, s_E) = 0, \tag{16}$$

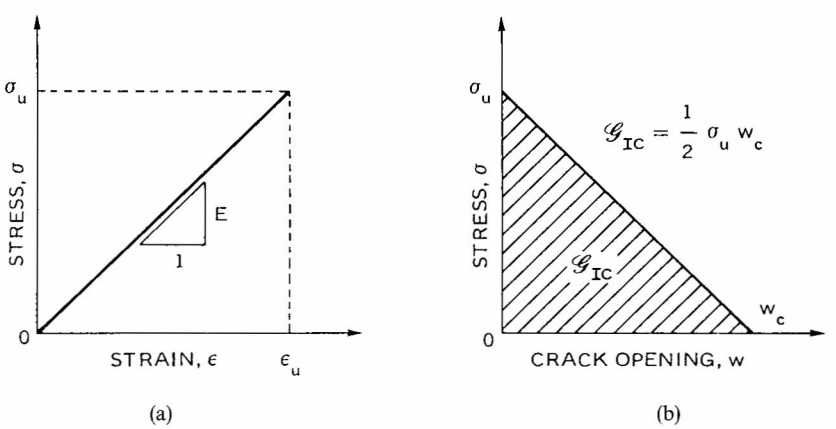

Fig. 4. Linear constitutive laws.

which corresponds to (4), if the *(energy) brittleness number*

$$s_E = \frac{\mathcal{G}_{IC}}{\sigma_u b}, \tag{17}$$

is introduced, as proposed by the writer [9–15].

When $n = 1$, $I_n = 1$, (9) is the generalized form of the well-known LEFM relation

$$K_I = \sqrt{\mathcal{G}_I E}. \tag{18}$$

If the *(stress) brittleness number*, in the particular case of linear-elastic material, is defined as [1–7]

$$s = \frac{K_{IC}}{\sigma_u b^{1/2}}, \tag{19}$$

from (17), (18) and (19) it is easy to obtain [14]

$$s_E = \varepsilon_u s^2, \tag{20}$$

which is the special case of (11).

If we take into account the relation (20) between s and s_E, through the ultimate strain ε_u, it is possible to present (16) in the following final form:

$$\bar{\pi}(\tilde{P}, \tilde{\delta}; s, s_E) = 0, \tag{21}$$

with the influence of the Poisson ratio being negligible. It is the particular form of (12), for a material which exhibits linearity in the σ vs ε ascending stable stage.

2.3. *Three point bending geometry*

Based on the preceding sections, it is possible to state that in general, for linear or non-linear materials and arbitrary geometries, we have physical similitude and, therefore, the same $\tilde{P}$ vs. $\tilde{\delta}$ structural response only when both the brittleness numbers s^* and s_E^*, see (5) and (10), are unchanged.

On the other hand, in the particular case of linear material (Fig. 4) and three point bending geometry (Fig. 5), it was shown by the writer [13] that in order to have physical similitude, it is sufficient that the *(stress) brittleness number* s, see (19), remains unchanged. A numerical analysis based on the cohesive crack model and applied to the three point bending geometry is able to particularize (16) as follows [13]:

$$\pi\left(\tilde{P}, \tilde{\delta}; \nu, \frac{s_E}{\varepsilon_u}\right) = 0, \tag{22}$$

and therefore, from (20)

$$\pi(\tilde{P}, \tilde{\delta}; s) = 0, \tag{23}$$

the influence of the Poisson ratio again being negligible.

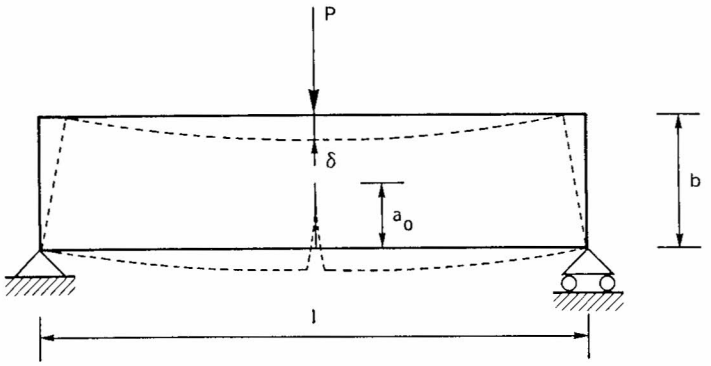

Fig. 5. Three point bending specimen.

If also the beam slenderness, $\lambda = l/b$, is involved in the analysis, (16) can take the form [13]

$$\pi\left(\tilde{P}, \tilde{\delta}; \nu, \frac{s_E}{\varepsilon_u \lambda}\right) = 0, \tag{24}$$

as is explained by a limit-analysis model proposed by the writer [11, 12], where the snap-back behaviour appears if

$$\frac{s_E}{\varepsilon_u \lambda} \lessapprox \frac{1}{3}. \tag{25}$$

When s_E is varied over four orders of magnitude, from 2×10^{-5} to 2×10^{-2}, completely different structural responses are represented in Fig. 6a for an intially uncracked

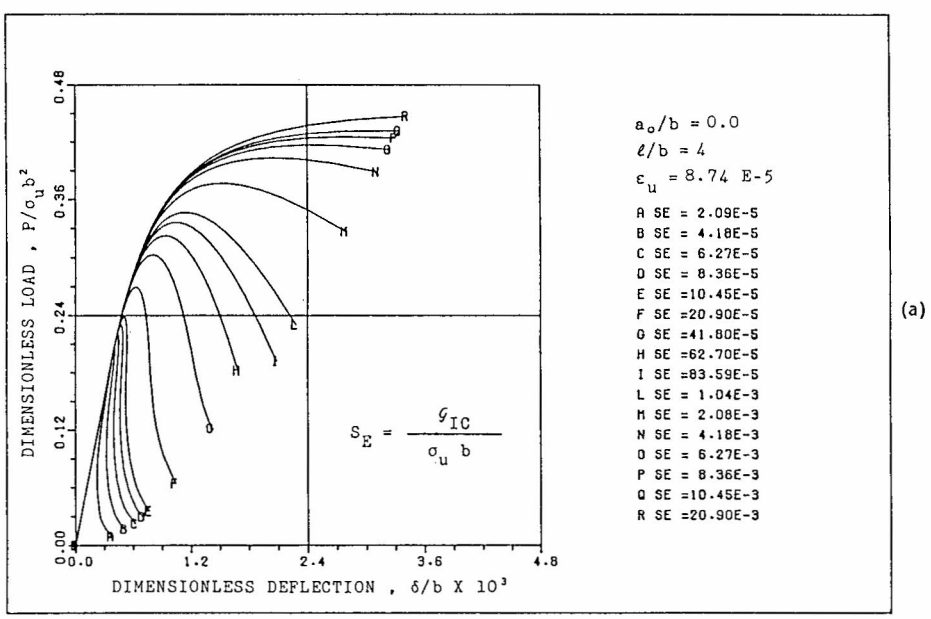

Fig. 6. Load vs. deflection diagrams by varying the energy brittleness number s_E.

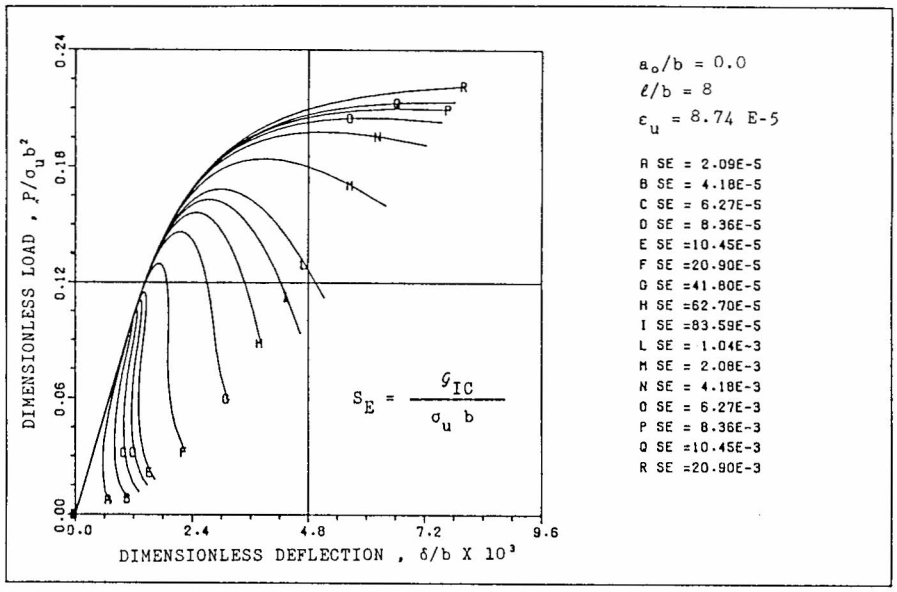

(b)

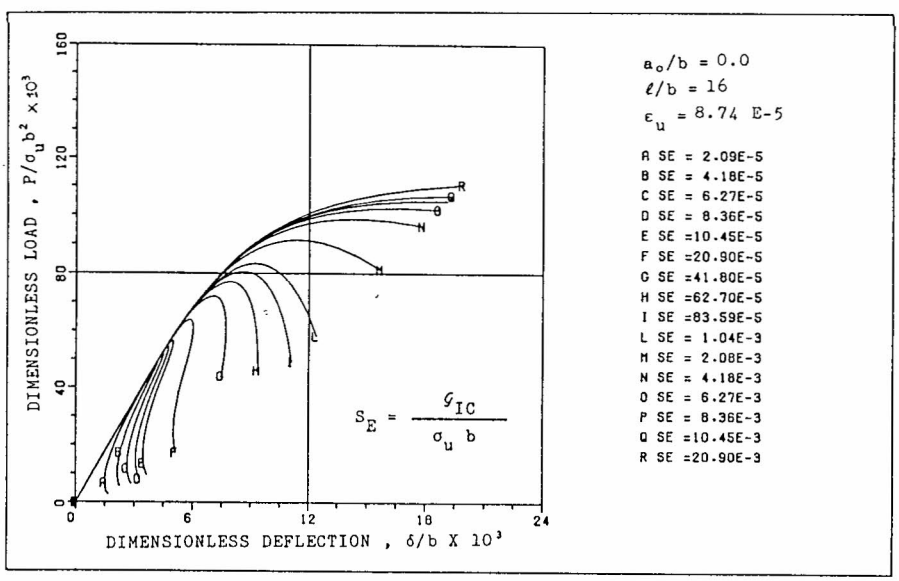

(c)

Fig. 6.—contd.

three point bending specimen, $a_0/b = 0.0$, of slenderness $\lambda = 4$, and an ultimate tensile strain $\varepsilon_u = 8.74 \times 10^{-5}$. The snap-back behaviour is predicted for $s_E \lesssim 10.45 \times 10^{-5}$, and then for

$$\frac{s_E}{\varepsilon_u \lambda} \lesssim \frac{1}{3.34}, \tag{26}$$

which is very close to the preceding approximate condition (25).

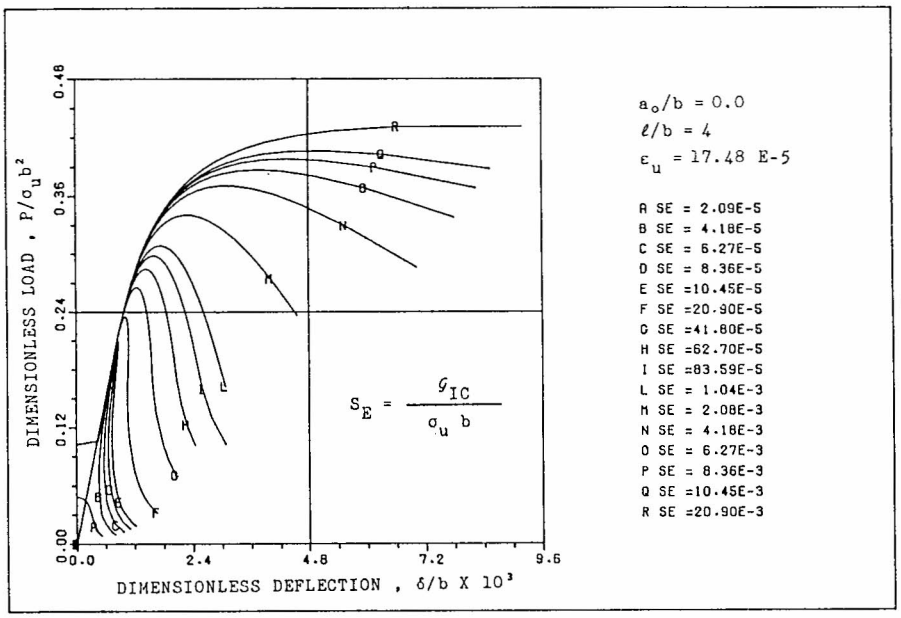

(d)

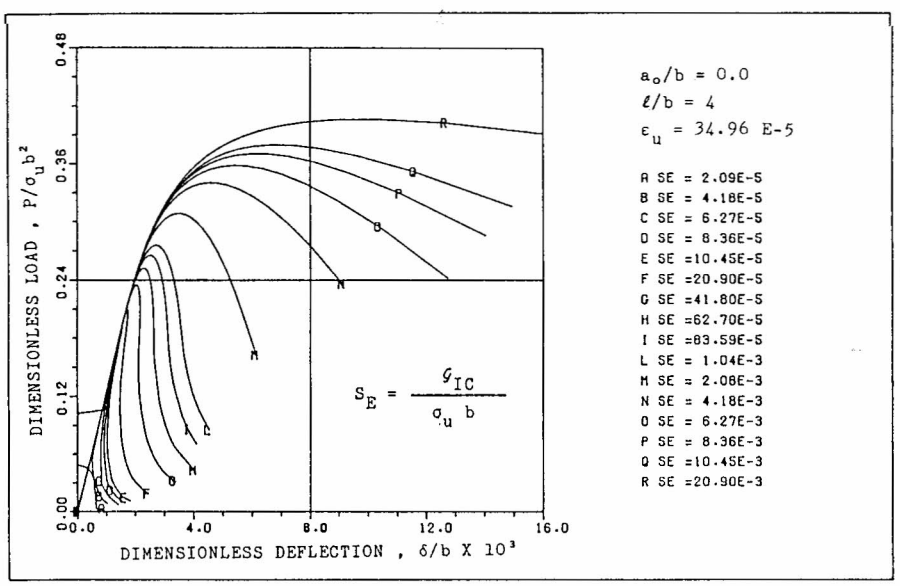

(e)

Fig. 6—contd.

The same variation of s_E is proposed in Fig. 6b, with $\lambda = 8$ and $\varepsilon_u = 8.74 \times 10^{-5}$. The snap-back behaviour is predicted for $s_E \lesseqgtr 20.90 \times 10^{-5}$, and then (26) is still valid. In Fig. 6c, with $\lambda = 16$ and $\varepsilon_u = 8.74 \times 10^{-5}$, the snap-back behaviour is predicted for $s_E \lesseqgtr 41.80 \times 10^{-5}$, and (26) is recovered once again.

In Figs. 6d and e, we have $\lambda = 4$ and ε_u respectively equal to 17.48×10^{-5} and 34.96×10^{-5}. In both cases condition (26) holds.

Recent experimental investigations on three point bending specimens of high strength concrete [26], brick [27] and rock [28] have confirmed the previous theoretical results. The extrapolation to mixed mode crack propagation in concrete was also considered [29, 30].

3. Scale effect on the J-resistance curve

The functional relationship between current value of the J-integral and relative crack length, is usually called the *J-resistance curve* and can be put into the following dimensionless form [22]

$$\Gamma\left(\frac{J_I}{\sigma_y b}, \frac{a}{b}; \varepsilon_y, n, n'; \xi_i\right) = 0, \tag{27}$$

where a is the current value of crack length. When J_I reaches its critical value J_{IC}, the crack propagation becomes fast and uncontrollable.

Usually, at the beginning of the slow and stable crack growth, the J_I vs. a relationship is an increasing function and can be considered as linear

$$\frac{J_I}{\sigma_y b} = \left(\frac{dJ_I/da}{\sigma_y}\right)\frac{a - a_0}{b} + \frac{J_0}{\sigma_y b}, \tag{28}$$

where $(dJ_1/|da)$ is the constant slope, J_0 the intercept on the J_1-axis and a_0 is the initial crack length. Equation (28) can obviously be rearranged into the form [22]

$$\tilde{J} = \tilde{J}'(\xi - \xi_0) + \tilde{J}_0, \tag{29}$$

where $\tilde{J}$ is the dimensionless J-integral and ξ is the relative crack length (Fig. 7). The constants $\tilde{J}'$ and $\tilde{J}_0$ are dimensionless and scale-independent. It follows that the slope of the J_I vs. a diagram is constant varying the scale, i.e. dJ_I/da = constant, and that the intercept J_0 is proportional to the size b. An experimental confirmation is found in [31].

On the basis of the previous assumptions, it is possible to state that above the size (Fig. 7)

$$b_{max} = \frac{J_{IC}}{\sigma_y \tilde{J}_0}, \tag{30}$$

stable crack growth ceases to occur and the brittle failure is achieved when the P vs δ curve is still in its linear course, whereas, below the size

$$b_{min} = \frac{J_{IC}}{\sigma_y[\tilde{J}_0 + \tilde{J}'(1 - \xi_0)]}, \tag{31}$$

unstable crack growth ceases to occur and the progressive slow crack growth develops up to the complete specimen separation. On the other hand, for $b_{min} < b < b_{max}$, stable (or slow) crack growth is followed by unstable (or fast) crack propagation. Even according to the J-resistance

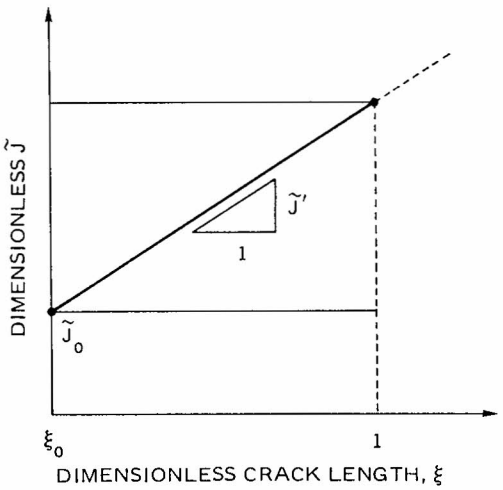

Fig. 7. Scale-invariant J-resistance curve.

approach, ductility or brittleness appears as a structural property rather than a material property.

Recalling the definition of (*energy*) *brittleness number* s_E^*, see (5), we can define a transitional interval between ductility and brittleness, following (30) and (31)

$$s_E^* \lessapprox \tilde{J}_0 \text{ (brittleness)}, \tag{32a}$$

$$\tilde{J}_0 \lessapprox s_E^* \lessapprox [\tilde{J}_0 + \tilde{J}'(1 - \xi_0)] \quad \text{(transitional interval)}, \tag{32b}$$

$$s_E^* \gtrapprox [\tilde{J}_0 + \tilde{J}'(\xi - \xi_0)] \quad \text{(ductility)}. \tag{32c}$$

Conditions (32) may correspond respectively to cusp-catastrophe, snap-back behaviour and strain-softening behaviour (Fig. 3).

4. Conclusions

1. A relationship between *stress brittleness number* (s^*) and *energy brittleness number* (s_E^*) is obtained (11) when both σ vs. ε and σ vs. w constitutive laws are non-linear. Each number is derivable from the other, once the ultimate strain ε_y and Ramberg-Osgood exponent n are known.
2. The structural response in the dimensionless plane $\tilde{P} - \tilde{\delta}$ depends on both the brittleness numbers s^* and s_E^*.
3. In the particular case of a linear elastic material and a three point bending geometry, the structural response depends only on the stress brittleness number s, if the geometrical ratios are fixed. Otherwise, it depends on the number $s_E/\varepsilon_u\lambda$, where λ is the beam slenderness.
4. The size-scale transition from ductile to brittle failure is captured also by the J-resistance approach. The relevant parameters of a scale-invariant J-resistance curve can be related to the energy brittleness number s_E^*, (32).

References

1. A. Carpinteri, in *Proceedings of the International Conference on Analytical and Experimental Fracture Mechanics*, Sijthoff and Noordhoff, Rome (1980) 785–797.
2. A. Carpinteri, *RILEM Materials and Structures* 14 (1981) 151–162.
3. A. Carpinteri, *Engineering Fracture Mechanics* 16 (1982) 467–481.
4. A. Carpinteri, *ASCE Journal of the Structural Division* 108 (1982) 833–848.
5. A. Carpinteri, C. Marega and A. Savadori, *Journal of Materials Science* 21 (1986) 4173–4178.
6. A. Carpinteri, *Engineering Fracture Mechanics* 26 (1987) 143–155.
7. A. Carpinteri, *Engineering Fracture Mechanics* 32 (1989) 265–278.
8. A. Carpinteri, *RILEM Materials and Structures* 16 (1983) 85–96.
9. A. Carpinteri, in NATO *Advanced Research Workshop on Applications of Fracture Mechanics to Cementitious Composites*, Martinus Nijhoff (1984) 287–316.
10. A. Carpinteri, *Journal of the Mechanics and Physics of Solids* 37 (1989) 567–582.
11. A. Carpinteri, *International Journal of Solids and Structures* 25 (1989) 407–429.
12. A. Carpinteri, *ASCE Journal of Engineering Mechanics* 115 (1989) 1375–1392.
13. A. Carpinteri and G. Colombo, *Computers and Structures* 31 (1989) 607–636.
14. A. Carpinteri, *International Journal for Numerical Methods in Engineering* 28 (1989) 1521–1537.
15. A. Carpinteri, *International Journal of Fracture* 44 (1990) 57–69.
16. A. Carpinteri, *ASCE Journal of Structural Engineering* 110 (1984) 544–558.
17. A. Carpinteri, *Magazine of Concrete Research* 40 (1988) 209–215.
18. C. Bosco, A. Carpinteri and P.G. Debernardi, *ASCE Journal of Structural Engineering* 116 (1990) 427–437.
19. C. Bosco, A. Carpinteri and P.G. Debernardi, *Engineering Fracture Mechanics* 35 (1990) 665–677.
20. Z.P. Bažant, *ASCE Journal of Engineering Mechanics* 110 (1984) 518–535.
21. Z.P. Bažant and P.A. Pfeiffer, *ACI Journal of Materials* 85 (1987) 463–480.
22. A. Carpinteri and G.C. Sih, *Theoretical and Applied Fracture Mechanics* 1 (1984) 145–159.
23. J.R. Rice, *Journal of Applied Mechanics* 35 (1968) 379–386.
24. J.R. Rice and G.F. Rosengren, *Journal of the Mechanics and Physics of Solids* 16 (1968) 1–12.
25. J.W. Hutchinson, *Journal of the Mechanics and Physics of Solids* 16 (1968) 13–31.
26. L. Biolzi, S. Cangiano, G. Tognon and A. Carpinteri, *RILEM Materials and Structures* 22 (1989) 429–436.
27. P. Bocca, A. Carpinteri and S. Valente, *RILEM Materials and Structures* 22 (1989) 364–373.
28. P. Bocca and A. Carpinteri, *Engineering Fracture Mechanics* 35 (1990) 241–250.
29. E. Ballatore, A. Carpinteri, G. Ferrara and G. Melchiorri, *Engineering Fracture Mechanics* 35 (1990) 145–157.
30. P. Bocca, A. Carpinteri and S. Valente, *Engineering Fracture Mechanics* 35 (1990) 159–170.
31. J.R. Gordon and R.L. Jones, *Fatigue and Fracture of Engineering Materials and Structures* 12 (1989) 295–308.